HHS Public Access

Author manuscript

Neuron. Author manuscript; available in PMC 2020 September 04.

Published in final edited form as:

Neuron. 2019 September 04; 103(5): 878–890.e3. doi:10.1016/j.neuron.2019.05.045.

Neurovascular coupling in the dentate gyrus regulates adult hippocampal neurogenesis

Jia Shen[1,2], **Depeng Wang**[4], **Xinxing Wang**[2], **Shashank Gupta**[2], **Bhargav Ayloo**[2], **Song Wu**[3], **Paras Prasad**[5], **Qiaojie Xiong**[2,*], **Jun Xia**[4,*], **Shaoyu Ge**[2,6,*]

[1]The Program of Genetics, SUNY at Stony Brook, Stony Brook NY 11794, USA

[2]Department of Neurobiology & Behavior, SUNY at Stony Brook, Stony Brook NY 11794, USA

[3]Department of Applied Mathematics and Statistics, SUNY at Stony Brook, Stony Brook NY 11794, USA

[4]Department of Biomedical Engineering, University at Buffalo, State University of New York, Buffalo, New York 14260, USA

[5]Institute for Lasers, Photonics and Biophotonics and the Department of Chemistry, University at Buffalo, State University of New York, Buffalo, New York 14260, USA

[6]Lead contact

Summary

Newborn dentate granule cells (DGCs) are continuously generated in the adult brain. The mechanism underlying how the adult brain governs hippocampal neurogenesis remains poorly understood. In this study, we investigated how coupling of pre-existing neurons to the cerebrovascular system regulates hippocampal neurogenesis. Using a new *in vivo* imaging method in freely moving mice, we found that hippocampus-engaged behaviors, such as exploration in a novel environment, rapidly increased microvascular blood flow velocity in the dentate gyrus. Importantly, blocking this exploration-elevated blood flow dampened experience-induced hippocampal neurogenesis. By imaging the neurovascular niche in combination with chemogenetic manipulation, we revealed that pre-existing DGCs actively regulated microvascular blood flow. This neurovascular coupling was linked by parvalbumin-expressing interneurons, primarily through nitric oxide signaling. We further showed that insulin growth factor 1 signaling participated in functional hyperemia-induced neurogenesis. Together, our findings revealed a neurovascular coupling network that regulates experience-induced neurogenesis in the adult brain.

[*]Correspondence: qiaojie.xiong@stonybrook.edu (Q.X.), junxia@buffalo.edu (J.X.), and shaoyu.ge@stonybrook.edu (S. Ge).

Author Contributions: Conceptualization, J.S., Q.X., J.X., and S. Ge; Methodology, J.S., D.W., J.X., and S.Ge; Formal Analysis, J.S. and S.W.; Investigation, J.S., X.W., S. Gupta, and B.A.; Writing, J.S. and S.Ge produced the initial manuscript, and all others reviewed and commented the manuscript; Supervision, Q.X., J.X., and S. Ge; Funding Acquisition, J.S., P.P., Q.X., J.X., and S. Ge.

Declaration of Interest

The authors declare no competing interests.

eTOC Blurb

Metabolic mechanism may control adult neurogenesis. Shen et al. reveal exploration in an enriched environment elevates blood flow in the dentate gyrus. This exploration-induced hyperemia, under the control of dentate neural circuits, is necessary for experience-induced survival of newborn neurons.

Introduction

Several thousand new dentate granule cells (DGCs) are generated in the adult brain daily (Altman and Das, 1965, Cameron and McKay, 2001). However, less than half of these newborn DGCs integrate into the pre-existing dentate gyrus circuit and participate in hippocampal functioning (Kempermann et al., 1997, Gu et al., 2012, Sahay et al., 2011, Nakashiba et al., 2012, Kirschen et al., 2017). Furthermore, how the adult brain actively and precisely controls the number of functional newborn DGCs remains poorly understood.

Previous studies have used immunohistochemical, pharmacological, electrophysiological, and gene expression profiling approaches to show that new DGC generation, survival, and integration are controlled by intrinsic signals Over a decade ago, gamma-aminobutyric acid (GABA) receptor expression was discovered on neural progenitor cells in the adult brain (Ge et al., 2006, Overstreet Wadiche et al., 2005, Espósito et al., 2005). This initial finding motivated many subsequent studies, which elegantly revealed that a pre-existing neural circuit regulates different aspects of adult hippocampal neurogenesis, including the generation, survival, and integration of new DGCs However, how hippocampal networks actively regulate neurogenesis remains largely unknown.

Several studies have suggested that neural progenitors and newborn DGCs are physically adjacent to the vasculature in the dentate gyrus (Palmer et al., 2000, Sun et al., 2015) and the subventricular zone (Mirzadeh et al., 2008, Shen et al., 2008, Tavazoie et al., 2008). Furthermore, many vasculature-related factors such as insulin-like growth factor 1 (IGF-1), vascular endothelial growth factor (VEGF), basic fibroblast growth factor, epidermal growth factor (EGF), and brain-derived neurotrophic factor (BDNF) have been found to regulate hippocampal neurogenesis (Kempermann et al., 1997, Goncalves et al., 2016, Trejo et al., 2001, Rafii et al., 2016). Importantly, studies of the cortex and retina have shown that neural circuits actively control cerebral vascular hemodynamics in capillaries (Attwell et al., 2010). These pioneering studies led us to question whether pre-existing hippocampal neural circuits influence microvascular hemodynamics in the dentate gyrus to actively regulate hippocampal neurogenesis.

Blood flow plays an essential role in regulating microvascular fluid exchange. Indeed, increased blood flow increases microvascular filtration (Yuan and Rigor, 2010). Microvascular hemodynamics and their physiological significance are commonly quantified in terms of blood flow velocity. Furthermore, in the cortex, barely detectable dilations cause obvious changes in microvascular blood flow velocity as detected by two-photon imaging (Kleinfeld et al., 1998, O'Herron et al., 2016, Blinder et al., 2013), confirming the sensitivity of this parameter. Recently, scientists showed that blood flow velocity efficiently reflects

local microvascular dynamics and their role in regulating perceptual behaviors (O'Herron et al., 2016).

To determine whether hippocampus-engaged behaviors regulate hemodynamics, we established a novel imaging method to monitor blood flow in freely moving animals. We found that hippocampus-engaged exploration robustly elevated microvascular hyperemia in the dentate gyrus. Interestingly, suppression of this elevation by inhibiting neuronal nitric oxide synthesis (nNOS) disrupted exploration-induced hippocampal neurogenesis. Furthermore, parvalbumin (PV)-expressing neurons likely through NO signaling were essential to the exploration-induced elevation in microvascular hyperemia. Finally, we found that pre-existing DGCs actively regulated hippocampal neurogenesis through the PV-vasculature and IGF-1 pathway. Together, these results demonstrated that DGC-PV neuron-vasculature coupling is essential to the regulation of exploration-induced hippocampal neurogenesis.

Results

Hippocampus-engaged exploration induces microvascular functional hyperemia in the dentate gyrus

To determine the role of neurovascular coupling (Fig. 1A) in hippocampal neurogenesis, we established an imaging method that would enable us to monitor hippocampal microvascular hemodynamics in the dentate gyrus of freely behaving animals

We expressed green fluorescent protein (GFP) in the dentate gyrus using adeno-associated virus (AAV) followed by the implantation of a gradient refractive index (GRIN) lens on top of the DGC layer (Fig. 1B). Four weeks later, we imaged the dentate gyrus with a miniature microscope as previously described (Kirschen et al., 2017). The contrast of the optical signal between red blood cells (RBCs) and plasma allowed us to monitor the movement of RBCs through a given microvessel (Fig. 1C). We recorded the images of an area averaging 600 × 600 pixels (375 μm χ 375 μm) with a frame rate of at least 80 Hz to compute the blood flow velocity (Fig.1C and Video S1). Each pixel on the selected vessel was aligned across frames on a dynamic map (DMap), with the RBCs displayed as black and the plasma as white (Fig. 1C, see also Methods) (Wang et al., 2013). The plasma displayed a constant size across the captured frames, while the RBCs moved more in varying clusters within microvessels (Fig. 1D). Thus, blood flow velocity could be computed using the slope of the aligned plasma. The slope remained constant at baseline, suggesting that this was an accurate measure for reporting blood flow velocity (Fig. 1D).

We next examined whether microvascular hemodynamic activity responded to hippocampus-engaged behaviors and regulated hippocampal neurogenesis. Exploration in an enriched environment (EE) increases adult hippocampal neurogenesis primarily by promoting survival of newborn DGCs. Therefore, we examined whether EE exploration promoted hippocampal neurogenesis by regulating hemodynamics. To determine whether EE exploration altered blood flow velocity in the dentate gyrus, mice expressing GFP in DGCs were imaged using the system described above (Fig. 1B). As illustrated in Figure 1E, we first recorded microvascular blood flow from these mice in a cage with bedding only (home

cage, HC) to establish the baseline blood flow velocity. We then exposed these animals to EE with five objects to facilitate exploration. This revealed that relative to the HC condition, the first 10 min of EE exploration promptly and robustly increased blood flow velocity, which is termed hyperemia (Fig. 1F). Interestingly, the blood flow velocity returned to basal levels within approximately 1 h of EE exploration (Fig. 1F). This corresponds with what we have previously observed by measuring DGC activity (Kirschen et al., 2017) and suggests that DGCs play a prominent role in regulating hemodynamic activity. To examine whether the increased blood flow persisted in the same EE, we examined blood flow for 24 h. As expected, blood flow declined during the first hour. However, flow increased again during the second hour, albeit at a slightly lower amplitude than the first (Fig. S1A). This fluctuation recurred in the subsequent hours (Fig. S1B), suggesting that the hemodynamics persist under the same EE.

We next tested whether this hyperemia is associated with hippocampal-engaged behaviors. We first performed similar recordings in the auditory cortex, which is expected to be independent to EE exploration. We observed little change in the flow rate between HC and EE (Fig. S1D). We then evaluated whether flow changed in the dentate gyrus during non-hippocampus-engaged behaviors using an auditory-cued memory task (Phillips and LeDoux, 1992). As shown in Figure S1E–F, there was little difference in the flow rate between pre- and post- sound onset as well as before and during the stimulus session. We further verified the flow increase in the hippocampus by performing an additional hippocampus-engaged task, novel location recognition (Barker and Warburton, 2011). This revealed an increase in DGC Ca^{2+} transient frequency in the object zone (Fig. S2A & B). As expected, blood flow was also elevated in the object zone when compared to the open zone (Fig. S2C). Interestingly, interactions with the object in a novel location also increased blood flow velocity relative to interactions with a familiar one (Fig. S2D). Taken together, these results demonstrated that neurovascular coupling in the dentate gyrus likely occurs during hippocampus-engaged behaviors.

Suppression of exploration-induced hyperemia dampens experience-induced hippocampal neurogenesis

To determine whether exploration-induced hyperemia is necessary for experience-induced survival of newborn DGCs, we next attempted to block hyperemia. Neuron-derived nitric oxide (NO) activity induces cerebral hyperemia (Attwell et al., 2010, Lourenco et al., 2014, Mishra et al., 2016, Iadecola, 2017). NO production can be inhibited by blocking the neuronal isoform of nitric oxide synthase (nNOS) with the omega-nitro-L-arginine methyl ester (L-NAME) (Pfeiffer et al., 1996). Therefore, we evaluated how communication between the neural and vascular systems affects neurogenesis by suppressing neuronal NO signaling.

We first examined how L-NAME administration affected exploration-induced hyperemia in the dentate gyrus. We expressed a Ca^{2+} indicator, GCaMP6f, instead of GFP via delivery of an AAV to the dentate gyrus of adult mice (Fig. 2A). Four weeks after viral injection and lens implantation, visualization of fluorescent signals from these animals revealed that GCaM6f expression was sufficient to assess both Ca^{2+} events in DGCs and microvascular

blood flow velocity (Fig. 2B, see also Video S2). We then evaluated whether L-NAME administration abolished exploration-induced hyperemia in the dentate gyrus. L-NAME was administered for 24 hours via the drinking water (100 mg/kg), a dose and duration that was previously confirmed to inhibit nNOS *in vivo* (Nishijima et al., 2012). As expected, 10 min of EE sharply increased blood flow velocity relative to basal levels prior to L-NAME treatment (Fig. 2C). Importantly, L-NAME treatment robustly attenuated EE-induced elevation of blood flow velocity relative to pre-L-NAME levels (Fig. 2C). We also evaluated whether L-NAME treatment affected local network activity by determining the frequency of DGC Ca^{2+} events. L-NAME treatment did not affect the EE exploration-induced increase in DGC Ca^{2+} transient frequency (Fig. 2D, see also Fig. S2J & K) as previously shown (Kirschen et al., 2017). Furthermore, 24 h of L-NAME treatment did not affect baseline (HC) blood flow velocity in the dentate gyrus (Fig. S2H). Although the baseline Ca^{2+} transient rate varied substantially between the two consecutive days (pre- and post-L-NAME), this change was not statistically significant (Fig. S2I).

We next sought to determine the effects of L-NAME administration on newborn DGC survival. Newborn DGCs were labeled with a single 5-bromo-2'-deoxyuridine (BrdU, 10 μg/g, i.p.) injection (Fig. 2E). Three days after BrdU injection, a time at which most newborn DGCs are post-mitotic and become immature DGCs (Ge et al., 2006), mice received either regular or L-NAME-containing (100 mg/kg) water. One day later, these animals were housed in either HC or EE and continued to receive either regular or L-NAME water. To elicit the strongest effect from hippocampus-engaged exploration on hippocampal neurogenesis, we changed object type and location daily to retain environment novelty (Kirschen et al., 2017). Two weeks after BrdU injection, we analyzed the survival of BrdU+ DGCs. As expected, EE robustly increased the number of BrdU+ DGCs in control-treated mice (Fig. 2E). However, L-NAME administration substantially attenuated EE-induced BrdU+ DGC survival (Fig. 2E). We further assessed the expression of activated caspase-3 in the dentate gyrus to confirm that this change was due to apoptotic cell death (Fig. S3E). We also verified this observation by staining newborn DGCs with doublecortin (DCX), a marker for newborn neurons, in control- and L-NAME-treated animals. This revealed that EE increased the number of DCX+ cells relative to HC in the control group, but not the L-NAME group (Fig. 2F). To verify that the BrdU+ cells were neuroblasts or immature neurons, we co-labeled these sections with BrdU and DCX/NeuN. This revealed no detectable differences across the assessed four groups (Fig. S3A–B). To exclude the potential effect of L-NAME administration on neural progenitor cell proliferation, we administered L-NAME and a single BrdU injection on the same day and then quantified the number of BrdU+ cells 2 d or 4 d later (Fig. 2G and Fig. S3C). This revealed a trend towards more BrdU+ cells in the L-NAME-administered group, which is consistent with the role of nNOS in cell division; however, this increase was not statistically significant (Fig. 2G). Similarly, we confirmed this result with co-staining of BrdU and DCX (Fig. S3D).

To exclude any non-specific effects of this pharmacological inhibition (i.e. targeting other isoform of NOS), we employed a genetic approach to target nNOS using an AAV-based small hairpin RNA (shRNA). Briefly, we injected AAV-GFP-U6-m-NOS1-shRNA into the dentate gyrus of adult mice. Two weeks after viral infusion, we revealed that nNOS-shRNA substantially reduced nNOS expression relative to scramble-shRNA (control) (Fig. S3F).

Similar to our findings using pharmacological nNOS inhibition (Fig. 2E), we observed an abolishment of EE exploration-induced survival (Fig. S3G).

To examine any potential effects of L-NAME on hippocampus-engaged memory, we also performed a novel location recognition task following L-NAME treatment. We found that there was no obvious difference in discrimination compared to those prior to L-NAME treatment (Fig. S2E–G).

Thus, we successfully suppressed the exploration-induced elevation of microvascular blood flow by inhibiting nNOS. This suppression decreased the exploration-induced survival of newborn DGCs, suggesting a potential role of functional hyperemia in regulating hippocampal neurogenesis.

Parvalbumin-expressing neurons mediate exploration-induced functional hyperemia in the dentate gyrus through NO signaling

We next evaluated which population of nNOS-expressing neurons regulated exploration-induced hyperemia in the dentate gyrus. In the dentate gyrus, nNOS is primarily expressed by different subpopulations of GABAergic interneurons (Jinno and Kosaka, 2006). To verify this, we immunostained hippocampal tissues for nNOS expression. As expected, most nNOS + neurons expressed Glutamic Acid Decarboxylase (GAD), a GABAergic neuron marker (Jinno and Kosaka, 2006) (Fig. S4A&B). Recent studies, including our own, have suggested that parvalbumin (PV) GABAergic interneurons are one of the major neuronal populations that regulate newborn DGC generation and circuit integration in the adult brain (Song et al., 2012, Song et al., 2013, Alvarez et al., 2016, Ge et al., 2006). We observed that PV interneuron processes were adjacent to blood vessels (Fig. S4C), which hints at their interaction. Therefore, we evaluated whether NO-releasing PV interneurons regulate local hemodynamics during exploration. We first verified the co-expression of PV and nNOS by immunolabeling of hippocampal sections. This revealed that ~17% of PV interneurons expressed nNOS (Fig. 3A), consistent with previous reports (Jinno and Kosaka, 2006).

We then determined whether directly activating PV neurons could alter blood flow. We expressed hM3Dq (Gq), an excitatory DREADD (Designer Receptors Exclusively Activated by Designer Drug) tagged with mCherry, in PV neurons by co-injecting AAV-DIO-hM3Dq-mCherry with AAV-CaMKII-GFP (for blood flow imaging) into the dentate gyrus of adult PV-Cre mice (Fig. 3B). DIO-mCherry only was injected as a control. The AAV-mediated transgene expression was observed in ~90.3% of PV+ neurons (Fig. S4D), suggesting the sufficiency of this labeling method. Four weeks after the surgery, we monitored blood flow in the dentate gyrus using GFP signal as described in Fig. 1B–D. DREADD-expressing PV neurons were activated with the synthesized designer activator, clozapine-N-oxide (CNO, 1 mg/kg, i.p.; Fig. 3B) (Armbruster et al., 2007). Remarkably, CNO-induced activation of PV interneurons in the dentate gyrus robustly elevated blood flow velocity relative to saline-injected controls (Fig. 3C&E). This increased velocity persisted for approximately 1 hour, during which time CNO was expected to activate PV neurons via hM3Dq (Armbruster et al., 2007). Furthermore, CNO injection did not affect blood flow velocity in animals whose PV cells expressed mCherry alone (Fig. S4J). We next determined whether this blood flow increase was mediated specifically by the PV subpopulation that expressed nNOS. To test

this, the same mice received L-NAME for 24 h as described above. L-NAME administration attenuated the increase in blood flow velocity induced by PV neuronal activation (Fig. 3D–E). Note that a small difference in blood flow velocity between CNO/L-NAME- and saline-treated animals was still observed, although this was not significant. This suggests that another mechanism may mediate this regulation; however, further testing is required to confirm this possibility. We further verified this observation using the shRNA knockdown approach (Fig. S4E) by co-injecting the dentate gyrus of adult PV-Cre mice with AAV-DIO-hM3Dq and AAV-NOS1-shRNA. Consistent with the suppression of nNOS by L-NAME, the PV+ neuron activation showed little effect on blood flow rate after nNOS knockdown, whereas in mice injected with the control virus still had increased flow (Fig. S4F).

We next question whether activation of PV interneurons is necessary for the exploration-induced elevation of blood flow velocity. Using a paradigm similar to the DREADD-mediated PV interneuron activation illustrated in Figure 3B, we inhibited PV interneurons in the dentate gyrus by expressing hM4Di with AAV-DIO-hM4Di-mCherry. Following basal level recordings, we measured blood flow velocity in the dentate gyrus during EE exploration. Consistently, in saline-injected animals, EE increased blood flow velocity relative to the HC (Fig. 3F). Notably, in these animals, CNO injection abolished the EE exploration-induced elevation of blood flow velocity, suggesting that PV interneuron activity is necessary to the exploration-induced blood flow increase (Fig. 3F). To determine whether chemogenetic manipulation of PV neurons modulated NO production, we analyzed the nNOS expression by measuring fluorescence intensity in mice injected with AAV-DIO-hM3Dq, -hM4Di, or -mCherry 2 h after CNO treatment. The hM4Di group (PV neuron inhibition) had lower nNOS expression than both the mCherry only and hM3Dq (PV neuron activation) groups (Fig. S4K). There was also a trend towards an increase in hM3Dq mice compared to mCherry only; however, this change was not statistically significant. This might be due to a fluorescence saturation effect, which might require another measurement approach.

Hippocampal neurogenesis induced by PV+ neuron activation requires neurovascular coupling

Thus, dentate gyrus PV+ interneuron activity likely through NO signaling mediated the exploration-induced microvascular blood flow increase. These results suggested a scheme in which the PV interneuron-microvessel pathway mediates exploration-induced hippocampal neurogenesis. To test this hypothesis, we directly manipulated PV+ interneuron activity and examine the effects on hippocampal neurogenesis (Fig. 3B). Specifically, we expressed hM3Dq-mCherry (or -mCherry) with the DIO-AAV vector in the dentate gyrus of PV-Cre mice. Three weeks after viral labeling, we divided these injected mice into four groups and injected a single BrdU (10 μg/g, i.p.) to label newborn DGCs. In two of the groups, we expressed hM3Dq in PV+ neurons by administering CNO once per day beginning 3 days after BrdU labeling to activate PV+ neurons. One group received regular water, while the other received water containing L-NAME to inhibit nNOS. The other two groups received control virus (DIO-mCherry) and either with regular or L-NAME water (Fig. 3H). We delivered CNO to all animals to control the side effect (if any) on neurogenesis. Fourteen days after BrdU labeling, we sacrificed these animals and quantified the number of BrdU+

DGCs. We found that PV+ neuron activation via hM3Dq robustly increased the number of BrdU+ DGCs compared to the control (Fig. 3H, see also Fig. S4I), consistent with previous findings. Remarkably, L-NAME administration substantially attenuated the PV+ neuron activation-induced increase of BrdU+ DGCs (Fig. 3G–H). We verified these observations by knocking down nNOS-derived NO production genetically (Fig. S4G). Consistent with the findings from L-NAME-mediated inhibition, there were fewer BrdU+ cells compared to the control shRNA group after PV+ neuron activation (Fig. S4H). This suggested that PV+/nNOS+ neurovascular coupling mediated by NO signaling plays a key role in regulating newborn DGC survival.

DGCs regulate exploration-induced hyperemia in the dentate gyrus

In the adult brain, DGCs actively respond to hippocampus-engaged behaviors, and have been shown to be required for the experience-dependent survival of newborn DGCs (Tashiro et al., 2007, Kirschen et al., 2017). Thus, we investigated whether DGCs regulated microvascular hemodynamics in the dentate gyrus by activating PV neurons and subsequently impacting the survival of newborn DGCs.

We first chemogenetically activated DGCs and analyzed microvascular flow in the dentate gyrus (Fig. 4A & B). We expressed AAV-CaMKII-hM3Dq-mCherry in DGCs and activated these neurons with CNO (Fig. 4B). We co-injected the AAV-CaMKII-GCaMP6f to monitor DGC activity and blood flow. Four weeks after viral injection, at which time point all hM3Dq expressing cells are mature DGCs (Fig. S5F)(Rhee et al., 2016), we recorded both DGC and vascular activity. To establish a baseline, we first imaged for 10 min prior to CNO injection (Fig. 4C–D). To analyze how DGC activation affected vascular activity, we captured images of animals anesthetized with an increased level of isoflurane to produce a low Ca^{2+} signal baseline. We recorded for 40 min beginning 20 min after CNO injection (1 mg/kg, i.p.), during which time the DGC activation by hM3Dq-CNO was expected to be effective and stable (Armbruster et al., 2007). As expected, CNO injection substantially increased the frequency of Ca^{2+} transients in DGCs (Fig. 4C). Notably, elevated neuronal activity coincided with increased local blood flow in the microvessels (Fig. 4D). In contrast, when we expressed the hM4Di to inhibit DGC activity, CNO (5 mg/kg, i.p.) suppressed the frequency of Ca^{2+} transients in DGCs, which coincided with decreased microvascular blood velocity (Fig. 4E–F). To facilitate this analysis, we decreased the isoflurane level to generate a high DGC activity baseline. To eliminate the possibility of systematic changes in blood flow, we also monitored heart rate during all recording sessions and found no detectable differences in the heart rate between CNO or saline injections (Fig. S5A).

We next determined whether DGC activity was required for exploration-induced hyperemia. We suppressed DGC activity using hM4Di expression and monitored this using the GCaMP6f (Fig. 5A–B). Similar to the procedure in Figure 3A, we recorded basal activity for 10 min before CNO delivery and then allowed the mice to explore in EE for 10 min. As shown in Figure 5C–D, EE exploration sharply increased the frequency of Ca^{2+} transients, similar to our previous observations (Kirschen et al., 2017). In the control group (saline), EE exploration also increased microvascular blood flow. Importantly, CNO attenuated the immediate elevation of DGC activity in EE (Fig. 5C–D). Interestingly, we found that

activating hM4Di in the dentate gyrus during EE exploration also significantly attenuated the increase in blood flow (Fig. 5E–F). In these experiments, we also compared the total locomotion between the two treatment groups and observed no obvious differences (Fig. S5B–E).

To further explore the effect of local microcircuits (DGC-PV) on blood flow, we evaluated whether PV neuron silencing affected DGC activation-induced hyperemia. We co-injected PV-Cre animals with AAV-CaMKII-hM3Dq and AAV-DIO-hM4Di (Fig. 5G), in which CNO treatment activates DGCs but silences PV neurons. We found that upon CNO administration, PV neuron inhibition sharply attenuated DGC activation-induced blood flow (Fig. 5H).

IGF-1R modulates neurovascular coupling-induced hippocampal neurogenesis

We next explored how functional hyperemia affected hippocampal neurogenesis. Several growth factors, including IGF-1, VEGF, and BDNF have been shown to regulate hippocampal neurogenesis (van Praag, 2008, Rafii et al., 2016). Furthermore, recent evidence has suggested that blood-borne IGF-1 crosses the blood brain barrier in the adult dentate gyrus to regulate neurogenesis (Åberg et al., 2000, PERT et al., 1988, Trejo et al., 2001, Nieto-Estevez et al., 2016). We therefore examined whether the IGF-1 signaling pathway was activated during EE exploration by staining hippocampal sections with an anti-phosphorylated IGF-1 receptor (pIGF-1R) antibody. We found that 14-day of EE exploration sharply increased the activation of IGF-1R in the inner granule cell layer. Importantly, nNOS inhibition by L-NAME, which suppresses functional hyperemia (Fig. 2), dampened the EE-induced IGF-1R activation (Fig. 6A). Note that L-NAME showed no statistically significant effect on baseline (in HC) IGF-1R activation.

We then evaluated whether IGF-1 signaling modulated EE-induced neurogenesis. We inhibited the IGF-1R by local infusion of picropodophyllin (PPP, 2.5 μM in DMSO), an IGF-1R antagonist, into the dentate gyrus. We first found that IGF-1R inhibition attenuated the EE exploration-induced survival of newborn DGCs (Fig. 6B & C), suggesting that IGF-1 signaling pathway may primarily regulate activity-dependent neurogenesis. Importantly, this antagonist had no visible effects on baseline neurogenesis in the HC (Fig. 6C). We then tested whether IGF-1 signaling is necessary for PV neuron activation-induced neurogenesis. In a cohort of PV-Cre mice injected with AAV-DIO-hM3Dq, we found that PPP infusion attenuated PV activity-induced newborn DGC survival (Fig. 6B & D). To exclude any effect of PPP on neural network activity in the dentate gyrus, we performed *in vivo* tetrode recording. This showed that PPP infusion had little effect on both DGC and interneuron activity compared with the control (Fig. S6).

Together, these results suggested that IGF-1 signaling was involved in PV-vasculature-induced neurogenesis. Thus, DGCs likely regulate exploration-induced changes in microvascular hemodynamics by activating PV neurons, and the microvasculature may regulate neurogenesis at least partially through IGF-1 signaling (Fig. 6E & F).

Discussion

The role of microvascular hemodynamics in adult hippocampal neurogenesis

The dynamics of newborn DGC development may be highly dependent on energy availability, which would require a constant blood supply from the vasculature. Indeed, several studies have previously hinted that hippocampal neurogenesis is regulated by the vasculature. A group of neurotrophic and growth factors released from the vasculature have been found to promote hippocampal neurogenesis, and neural progenitors are associated with the vascular niche. However, it is suggested that angiogenesis is not required for activity-dependent hippocampal neurogenesis (Pereira et al., 2007). Additionally, others have shown that neuronal activity drives the local vasculature to transport serum IGF-1 into local brain circuits (Nishijima et al., 2010, Carro et al., 2001). These findings hinted that hemodynamics, rather than angiogenesis, respond to hippocampus-engaged behaviors. In this investigation, our results suggested that hippocampus-engaged behaviors elevate blood flow locally, likely to provide more oxygen and neurotropic factors to the dentate gyrus. However, it remains interesting to explore whether other blood-borne factors are also involved in this regulation.

A recent study showed that radial glia-like progenitors ensheathe the vasculature in the inner molecular layer (Moss et al., 2016). This raises another possibility that functional hyperemia may also impact proliferation and differentiation of radial glia-like cells. However, whether this regulation is also via interneuron activation or whether DGCs play a similar role as that in the survival regulation remain to be tested.

Functional hyperemia during hippocampus-engaged behaviors

For consistent data acquisition and animal handling, most experiments were performed during the daytime. The EE exploration-induced increase of microvascular blood flow exhibited an interesting rhythmic dynamic instead of short-term habituation (Fig. S1A–C). Notably, when we extended the recording window to 24 h, we observed a sharp increase in blood flow velocity during the nighttime, which is consistent with previous observation of larger effects on neurogenesis with nighttime interventions (Holmes et al., 2004). In this study, our brief novel location recognition testing indicated that other hippocampus-engaged behaviors may drive similar hemodynamics to regulate neurogenesis, as previously reported. However, whether the adult hippocampus employs similar mechanisms to control different hippocampus task-induced neurogenesis requires further examination.

NO signaling mediates neurovascular coupling, but not DGC activity, in the dentate gyrus

Several studies, mainly in the cortex, have shown that NO release from active neurons regulates vascular hemodynamics by directly targeting the vasculature (Mishra et al., 2016, Lindauer et al., 1999). In this study, we assessed blood flow in the microvessels (~10 μm) surrounding DGCs to evaluate local vascular hemodynamics. We found that NO signaling played a key role in mediating the exploration-induced flow increase. Although how NO regulates blood flow remains underdetermined, one possibility is that NO acts on the upstream arterioles by relaxing smooth muscles or directly on capillary pericytes. Alternatively, other studies have shown that in response to glutamate, reactive astrocytes

impact vascular hemodynamics. From their endfeet, astrocytes release various vasodilators onto the smooth muscle on arterioles (Zonta et al., 2003, Mulligan and MacVicar, 2004). In contrast, a recent study suggested that astrocytes might act on capillary pericytes but not arterioles (Mishra et al., 2016). Future studies are required to determine whether and how astrocytes mediate vasodilation in the dentate gyrus.

Mounting evidence has shown that NO signaling modulates many biological functions such as cell division and synaptic plasticity. *In vitro,* nNOS limits the proliferation and differentiation of neural stem cells (Luo and Zhu, 2010). In the rat brain, blocking NO by intraventricular infusion of a NO synthase inhibitor promotes neurogenesis (Packer et al., 2003). Furthermore, neural stem cell-derived nNOS may be necessary for proliferation and differentiation of these cells, while extracellular-derived NO has the opposite effect (Luo et al., 2010). Indeed, how the NO signaling precisely regulates cell development in various conditions and brain regions need to be further studied. In this study, we found that there was a trend towards an increased number of BrdU+ cells in the HC group with L-NAME, but it was not statistically significant (Fig. 2G). For the survival experiments, we have inhibited nNOS from 3 days after BrdU labeling, at which time point we expect most labeled cells were postmitotic (i.e. DCX+). We thus expect that the effect was largely from its impact on the survival of newborn DGCs.

Neural circuit activity and vascular hemodynamics

Recent studies have revealed that GABAergic signaling, mainly from PV interneurons, critically regulates DGC generation, survival, and integration through conventional synaptic or non-synaptic transmission (Alvarez et al., 2016, Ge et al., 2006, Song et al., 2013, Esposito et al., 2005, Wadiche et al., 2005). Although these experiments provided elegant findings, how newborn DGCs could dynamically receive nutrition corresponding to GABAergic inputs remained unclear. Here, we found that PV+/nNOS+ neurons in the dentate gyrus regulated microvascular hemodynamics and might subsequently enhance newborn DGC survival.

In conclusion, using a newly established imaging method, we identified a novel pathway by which hippocampus-engaged exploration regulates hippocampal neurogenesis via neurovascular coupling in the dentate gyrus. These findings not only advance our understanding of the mechanisms underlying experience-dependent neurogenesis, but also enhance our understanding of how the adult brain actively governs its metabolic homeostasis.

STAR Methods

CONTACT FOR REAGENT AND RESOURCE SHARING

Further information and requests for resources and reagents should be directed to and will be fulfilled by the Lead Contact, Shaoyu Ge (shaoyu.ge@stonybrook.edu)

METHOD DETAILS

Animal and virus—The Stony Brook University IACUC-monitored Division of Laboratory Animal Resources maintained all animals. All surgeries and experimental procedures were reviewed and approved by the Stony Brook University Animal Use Committee and followed the guidelines of the National Institutes of Health. C57BL/6, for all wildtype control (Charles River Laboratories) and PV-Cre transgenic mice, in which PV promotor/enhancer drives Cre recombinase (Jackson Laboratory, stock# 017320) were used in this study. Surgeries were conducted using 6- to 8- week-old mice and Each dataset included both male and female animals, as previous work has shown no detectable sex differences in adult hippocampal neurogenesis (Lagace et al., 2007; Ben Abdallah et al., 2010). All mice were housed in pairs and maintained on a 12-h light/dark cycle. All behavioral experiments were performed during the light cycle. Mice were provided ad libitum access to food and water.

Adeno-associated virus 9 (AAV9)-calmodulin protein kinase II (CaMKII)-GCaMP6f was purchased from the University of Pennsylvania Vector Core. AAV8-CaMKII-EGFP, AAV8-CaMKII-hM3Dq-mCherry, -hM4Di-mCherry and -mCherry were purchased from Addgene (Watertown, MA). The Cre recombinant-dependent DIO-AAV (a double-floxed of open reading frame AAV) DREADDs AAV8-hSyn-DIO -hM3Dq-mCherry, -hM4Di-mCherry, and -mCherry were also purchased from Addgene. The shRNA viruses, AAV8-GFP-U6-m-NOS1-shRNA, in which targets the mouse NOS1, and AAV8-GFP-U6-Scrmb-shRNA (scrambled shRNA), were purchased from VECTOR BIOLABS (Malvern, PA).

In vivo simultaneous imaging—AAV9-CaMKII-GCaMP6f virus (University of Pennsylvania Vector Core) was stereotaxically injected into the dorsal dentate gyrus as previously described (Gu et al., 2012). In brief, mice were anesthetized with ketamine/Xylazine cocktail. The virus was injected at 1.5 mm depth −2.0 mm of bregma, and 1.6 mm lateral to the midline. This region was selected given the critical role of the dorsal hippocampus in spatial navigation (Moser and Moser, 1998; Hampson et al., 1999). After about one week of viral expression, a lens probe (outer diameter 1.0 mm, length = 4.0 mm, numerical aperture = 0.5) was implanted ~200 μm above the DGC layer. About 3 weeks later, a microscope baseplate was fixed to an optimized focal plane on top of the lens probe. All Ca^{2+}/blood flow imaging videos were recorded using a miniature microscope and the nVista data acquisition system (Inscopix, Palo Alto, CA) at a frame rate of 80-100 Hz. For the DGC neurovascular coupling verifying experiments (Fig. 4), Ca^{2+} imaging was performed with anesthetized mice (VetFlo, Kent Scientific Corp., Torrington, CT) with controlled heart rate (~450 bpm) and body temperature (36.5°C) (Mouse Stat, Kent Scientific Corp.). To successfully capture blood flow, we expressed GFP (GCaMP6f in Fig. 2, 4 and 5) in the dentate gyrus so that the fluorophore excitation could generate a background illumination on the blood vessel. This created a sharp contrast in RBCs and plasma due to their difference in fluorescent absorption.

Data processing and analysis—The Ca^{2+} signal was processed as previously described (Kirschen et al., 2017). Briefly, videos taken from the same animals with the same field of view (FOV) were concatenated and motion-corrected (Mosaic, Inscopix) Then, active cells

were detected by a combined principle component–independent component analysis algorithm (Mukamel et al., 2009) with a 0.1 weight of temporal information. Individual cells detected by the algorithm were screened manually from each concatenated video. Only cells with clearly identified signals were included. Ca^{2+} events were identified by a criterion of 8 as the median absolute deviation and a 0.2 s tau-off with the input-normalized dF/F signal at its local maximum. Changes in the z-axis, associated with a rotation in the microscope's FOV (i.e., rotation of the sensor turret), were not observed.

Blood flow velocity in the microvessels was analyzed in Matlab with the processed videos exported from Mosaic. The Matlab-based algorithm extracts each pixel within the selected vessel and replots them over time on a DMap. In the DMap, the x-axis represents time and the y-axis represents the pixel number along the vessel. Because the background green fluorescence is strongly absorbed by RBCs but not the blood plasma, each episode of plasma crossing the vessel forms a white stripe on the DMap. The slope of each white stripe indicates the speed of one unit of RBC moving across the selected vessel at that moment (Wang et al., 2013). Velocity (μm/s) was calculated as: slope*fps/1.6. Here, fps represents frames per second and 1.6 is the pixel/μm ratio of the recording setting. The blood flow velocity at a given minute was calculated by averaging the slopes of all detectable plasma white stripes. For the simultaneous imaging in EE, we averaged the measurements over a 3-min time window (i.e. EE 1 = 1-3 min after exposure) due to variations in neuronal activity during free exploration.

Behaviors

EE exploration: For EE exploration experiments, imaging was performed on freely behaving mice in HC to establish a baseline. Then, mice were moved to the EE (with about 5 objects) and allowed to freely explore. EE did not include any running wheels. Imaging was performed for either 10 min or 1 h of EE exploration. In the DREADD studies, mice generally received either saline or CNO (i.p.) 30 min prior to EE. Some exceptions have been specifically addressed in the results.

Auditory stimulus task: Mice were allowed to habituate to the recording chamber for two days (30 min per day). On the following day, baseline blood flow was recorded first (1 min in the chamber). The auditory stimulus (5 – 40 kHz tone cloud, 0.2 s each) was then randomly played in a 5 – 10 s interval for 5 min.

Novel location recognition: Mice were allowed to habituate to the recording room and an open field for three consecutive days (5 min per day)(Leger et al., 2013) before the experiment. One day 1 (familiarization day), animals were exposed to two novel objects in the open field. Twenty-four hours later (test day), animals were placed back to the same field with the same objects, but one was moved to a novel location. For the L-NAME study, this procedure was repeated on day 3 and 4 with a different set of objects. Each exploration session lasted 10 min. The animal behavior was recorded and analyzed by EthoVision 12.0 (Noldus Information Technology Inc.).

Pharmacological studies: 5-bromo-2'-deoxyuridine (BrdU, Sigma) was dissolved in sterile saline (10 mg/ml) and all neurogenesis experiments were from a single intraperitoneal injection (10 μg/g). Clozapine-N-oxide (CNO, Enzo Life Sciences, Inc., Farmingdale, NY) was dissolved in Milli-Q water to a final concentration of 5 mg/L and delivered to the mice at 1 mg/kg (i.p.) for hM3Dq and 5 mg/kg for hM4Di. The N omega-nitro-L-arginine methyl ester (L-NAME; Sigma-Aldrich, St. Louis, MO) was dissolved in the drinking water at 100 mg/kg. Water bottles were covered in foil to prevent light degradation. Picropodophyllotoxin (PPP, Cayman Chemical Company, Ann Arbor, MI) was dissolved in DMSO to a final concentration of 2.5 μM and was infused into the dentate gyrus at 200 nl/day.

Immunofluorescence staining and histology: Mice were deeply anesthetized with urethane (200 μg/g) and perfused transcardially with phosphate-buffered saline (PBS) and then 4% paraformaldehyde (PFA). Brains were removed, fixed overnight in 4% PFA, transferred to a 30% (w/v) sucrose solution, and stored at 4°C until sectioning. Brains were sectioned into 60-μm coronal sections over the entire anterior–posterior axis of the dentate gyrus. Immunohistochemistry was performed by blocking sections in 1% donkey serum in PBS + 0.025% Triton for 1 h at room temperature (after incubation in 2 N HCl for 25 min at 37°C for BrdU only). Sections were th en switched to primary antibodies, including BrdU (rat monoclonal antibody, 1:500; Abcam, Cambridge, MA), doublecortin (goat polyclonal antibody, 1:1000; Santa Cruz Biotechnology, Dallas, TX), NOS1 (mouse monoclonal antibody, 1:100; Santa Cruz), parvalbumin (rabbit polyclonal antibody, 1:1000; Abcam, Cambridge, UK), NeuN (mouse monoclonal antibody, 1:500; Millipore Sigma), CD31 (rat monoclonal antibody, 1:200; BD Biosciences, San Jose, CA) and activated caspase-3 (1:100; Cell Signaling), for overnight shaking at 4°C. Sections were then switch ed to secondary antibodies, including Alexa Fluor 488-conjugated donkey anti-rat, anti-rabbit, anti-mouse antibody (1:1000; Abcam) and Alexa Fluor 594-conjugated donkey anti-goat antibody (1:500; Abcam), for 3 h shaking at room temperature. Images were obtained on an Olympus FLV1000 confocal microscope. We used every fourth brain section and counted fluorescently labeled cells within the granule cell layer and sub-granular zone for half of the brain across the entire anterior–posterior axis of the dentate gyrus. We then multiplied this number by two to approximate the total number of labeled cells/dentate gyrus as described previously (Gould et al., 1999; Cameron and McKay, 2001). For the brains collected from the imaging experiments, the lens probe implantation sites were inspected to confirm the location (200-300 μm above the granule cell layer).

QUANTIFICATION AND STATISTICAL ANALYSIS

We performed statistical tests as follows: Linear mixed model for longitudinal data (Fig. 1F, 2C&D, 3C, D, and F, 4C–F, 5D, F, and H, S1D, S1F, and S4J), two-way ANOVAs followed by post hoc Bonferroni's test or Kruskal-Wallis test for BrdU and DCX quantification, Wilcoxon's signed rank test (for paired measurement) or Mann-Whitney test (for unpaired measurement) for blood flow and Ca^{2+} transient rate bar plots, and Kolmogorov–Smirnov test for brain slice electrophysiology data. In the linear mixed model, the animal was treated as a random effect to model the correlation among measurements from the same mouse and normality assumption was confirmed. All analysis has been estimated with 95% confidence interval and *P*-values of 0.05 were considered the cutoff for statistical significance.

Statistical analysis was performed using SAS 9.4 (SAS institute Inc., Cary, NC). All data are represented as mean ± SEM. n represents the number of animals unless otherwise specified.

Supplementary Material

Refer to Web version on PubMed Central for supplementary material.

Acknowledgements:

This work was supported by the National Institutes of Health (Grants NS089770, AG046875, NS104868 to S.G., DC016746 to Q.X), the American Heart Association predoctoral fellowship (18PRE34080158 to J.S.), and partially by the SUNY Brain Network of Excellence. We thank Drs. Simon Halegoua, Hongjun Song, Linda Overstreet-Wadiche, and Greg Kirschen for their critical feedback on this manuscript; Alexandras Kokkosi and Dr. Stylianianna Tsirka for their help with cleaved caspase-3 immunostaining; Dr. Ignacio Torres for his help with IGF-1R inhibition experiment. We also thank all other members in the Ge and Xiong laboratories for their valuable comments.

References

ÅBERG MAI, ÅBERG ND, HEDBÄCKER H, OSCARSSON J & ERIKSSON PS 2000 Peripheral Infusion of IGF-I Selectively Induces Neurogenesis in the Adult Rat Hippocampus. The Journal of Neuroscience, 20, 2896–2903. [PubMed: 10751442]

ALTMAN J & DAS GD 1965 Autoradiographic and histological evidence of postnatal hippocampal neurogenesis in rats. J Comp Neurol, 124.

ALVAREZ DD, GIACOMINI D, YANG SM, TRINCHERO MF, TEMPRANA SG, BÜTTNER KA, BELTRAMONE N & SCHINDER AF 2016 A disynaptic feedback network activated by experience promotes the integration of new granule cells. Science, 354, 459. [PubMed: 27789840]

ARMBRUSTER BN, LI X, PAUSCH MH, HERLITZE S & ROTH BL 2007 Evolving the lock to fit the key to create a family of G protein-coupled receptors potently activated by an inert ligand. Proceedings of the National Academy of Sciences, 104, 5163–5168.

ATTWELL D, BUCHAN AM, CHARPAK S, LAURITZEN M, MACVICAR BA & NEWMAN EA 2010 Glial and neuronal control of brain blood flow. Nature, 468, 232–43. [PubMed: 21068832]

BARKER GR & WARBURTON EC 2011 When is the hippocampus involved in recognition memory? J Neurosci, 31, 10721–31. [PubMed: 21775615]

BLINDER P, TSAI PS, KAUFHOLD JP, KNUTSEN PM, SUHL H & KLEINFELD D 2013 The cortical angiome: an interconnected vascular network with noncolumnar patterns of blood flow. Nat Neurosci, 16, 889–97. [PubMed: 23749145]

CAMERON HA & MCKAY RD 2001 Adult neurogenesis produces a large pool of new granule cells in the dentate gyrus. J Comp Neurol, 435.

CARRO E, TREJO JL, BUSIGUINA S & TORRES-ALEMAN I 2001 Circulating Insulin-Like Growth Factor I Mediates the Protective Effects of Physical Exercise against Brain Insults of Different Etiology and Anatomy. The Journal of Neuroscience, 21, 5678–5684. [PubMed: 11466439]

ESPÓSITO MS, PIATTI VC, LAPLAGNE DA, MORGENSTERN NA, FERRARI CC, PITOSSI FJ & SCHINDER AF 2005 Neuronal Differentiation in the Adult Hippocampus Recapitulates Embryonic Development. The Journal of Neuroscience, 25, 10074. [PubMed: 16267214]

GE S, GOH EL, SAILOR KA, KITABATAKE Y, MING GL & SONG H 2006 GABA regulates synaptic integration of newly generated neurons in the adult brain. Nature, 439, 589–93. [PubMed: 16341203]

GONCALVES JT, SCHAFER ST & GAGE FH 2016 Adult Neurogenesis in the Hippocampus: From Stem Cells to Behavior. Cell, 167, 897–914. [PubMed: 27814520]

GU Y, ARRUDA-CARVALHO M, WANG J, JANOSCHKA SR, JOSSELYN SA, FRANKLAND PW & GE S 2012 Optical controlling reveals time-dependent roles for adult-born dentate granule cells. NatNeurosci, 15,1700–1706.

HOLMES MM, GALEA LA, MISTLBERGER RE & KEMPERMANN G 2004 Adult hippocampal neurogenesis and voluntary running activity: circadian and dose-dependent effects. J Neurosci Res, 76, 216–22. [PubMed: 15048919]

IADECOLA C 2017 The Neurovascular Unit Coming of Age: A Journey through Neurovascular Coupling in Health and Disease. Neuron, 96, 17–42. [PubMed: 28957666]

JINNO S & KOSAKA T 2006 Cellular architecture of the mouse hippocampus: a quantitative aspect of chemically defined GABAergic neurons with stereology. Neurosci Res, 56, 229–45. [PubMed: 16930755]

KEMPERMANN G, KUHN HG & GAGE FH 1997 More hippocampal neurons in adult mice living in an enriched environment. Nature, 386, 493–495. [PubMed: 9087407]

KIRSCHEN GW, SHEN J, TIAN M, SCHROEDER B, WANG J, MAN G, WU S & GE S 2017 Active Dentate Granule Cells Encode Experience to Promote the Addition of Adult-Born Hippocampal Neurons. The Journal of Neuroscience, 37, 4661. [PubMed: 28373391]

KLEINFELD D, MITRA PP, HELMCHEN F & DENK W 1998 Fluctuations and stimulus-induced changes in blood flow observed in individual capillaries in layers 2 through 4 of rat neocortex. Proceedings of the National Academy of Sciences, 95, 15741–15746.

LEGER M, QUIEDEVILLE A, BOUET V, HAELEWYN B, BOULOUARD M, SCHUMANN-BARD P & FRERET T 2013 Object recognition test in mice. Nat Protoc, 8, 2531–7. [PubMed: 24263092]

LINDAUER U, MEGOW D, MATSUDA H & DIRNAGL U 1999 Nitric oxide: a modulator, but not a mediator, of neurovascular coupling in rat somatosensory cortex. American Journal of Physiology-Heart and Circulatory Physiology, 277, H799–H811.

LOURENCO CF, SANTOS RM, BARBOSA RM, CADENAS E, RADI R & LARANJINHA J 2014 Neurovascular coupling in hippocampus is mediated via diffusion by neuronal-derived nitric oxide. Free Radic Biol Med, 73, 421–9. [PubMed: 24887095]

LUO CX, JIN X, CAO CC, ZHU MM, WANG B, CHANG L, ZHOU QG, WU HY & ZHU DY 2010 Bidirectional regulation of neurogenesis by neuronal nitric oxide synthase derived from neurons and neural stem cells. Stem Cells, 28, 2041–52. [PubMed: 20845474]

MIRZADEH Z, MERKLE FT, SORIANO-NAVARRO M, GARCIA-VERDUGO JM & ALVAREZ-BUYLLA A 2008 Neural stem cells confer unique pinwheel architecture to the ventricular surface in neurogenic regions of the adult brain. Cell Stem Cell, 3, 265–78. [PubMed: 18786414]

MISHRA A, REYNOLDS JP, CHEN Y, GOURINE AV, RUSAKOV DA & ATTWELL D 2016 Astrocytes mediate neurovascular signaling to capillary pericytes but not to arterioles. Nat Neurosci, 19, 1619–1627. [PubMed: 27775719]

MULLIGAN SJ & MACVICAR BA 2004 Calcium transients in astrocyte endfeet cause cerebrovascular constrictions. Nature, 431, 195. [PubMed: 15356633]

NAKASHIBA T, CUSHMAN JESSED, PELKEY KENNETHA, RENAUDINEAU S, BUHL DEREKL, MCHUGH THOMASJ, BARRERA VANESSAR, CHITTAJALLU R, IWAMOTO KEISUKES, MCBAIN CHRISJ, FANSELOW MICHAELS & TONEGAWA S 2012 Young Dentate Granule Cells Mediate Pattern Separation, whereas Old Granule Cells Facilitate Pattern Completion. Cell, 149, 188–201. [PubMed: 22365813]

NIETO-ESTEVEZ V, OUESLATI-MORALES CO, LI L, PICKEL J, MORALES AV & VICARIO-ABEJON C 2016 Brain Insulin-Like Growth Factor-I Directs the Transition from Stem Cells to Mature Neurons During Postnatal/Adult Hippocampal Neurogenesis. Stem Cells, 34, 2194–209. [PubMed: 27144663]

NISHIJIMA T, OKAMOTO M, MATSUI T, KITA I & SOYA H 2012 Hippocampal functional hyperemia mediated by NMDA receptor/NO signaling in rats during mild exercise. J Appl Physiol (1985), 112, 197–203. [PubMed: 21940846]

NISHIJIMA T, PIRIZ J, DUFLOT S, FERNANDEZ AM, GAITAN G, GOMEZ-PINEDO U, VERDUGO JM, LEROY F, SOYA H, NUNEZ A & TORRES-ALEMAN I 2010 Neuronal activity drives localized blood-brain-barrier transport of serum insulin-like growth factor-I into the CNS. Neuron, 67, 834–46. [PubMed: 20826314]

O'HERRON P, CHHATBAR PY, LEVY M, SHEN Z, SCHRAMM AE, LU Z & KARA P 2016 Neural correlates of single-vessel haemodynamic responses in vivo. Nature, 534, 378–82. [PubMed: 27281215]

OVERSTREET WADICHE L, BROMBERG DA, BENSEN AL & WESTBROOK GL 2005 GABAergic signaling to newborn neurons in dentate gyrus. J Neurophysiol, 94, 4528–32. [PubMed: 16033936]

PACKER MA, STASIV Y, BENRAISS A, CHMIELNICKI E, GRINBERG A, WESTPHAL H, GOLDMAN SA & ENIKOLOPOV G 2003 Nitric oxide negatively regulates mammalian adult neurogenesis. Proc Natl Acad Sci U S A, 100, 9566–71. [PubMed: 12886012]

PALMER TD, WILLHOITE AR & GAGE FH 2000 Vascular niche for adult hippocampal neurogenesis. The Journal of Comparative Neurology, 425, 479–494. [PubMed: 10975875]

PEREIRA AC, HUDDLESTON DE, BRICKMAN AM, SOSUNOV AA, HEN R, MCKHANN GM, SLOAN R, GAGE FH, BROWN TR & SMALL SA 2007 An in vivo correlate of exercise-induced neurogenesis in the adult dentate gyrus. Proceedings of the National Academy of Sciences, 104, 5638–5643.

PERT CB, ROTH J, HILL JM, ROJESKI M, LESNIAK MA & KIESS W 1988 Receptors for Insulin-like Growth Factors I and II: Autoradiographic Localization in Rat Brain and Comparison to Receptors for Insulin*. Endocrinology, 123, 2089–2099. [PubMed: 2970961]

PFEIFFER S, LEOPOLD E, SCHMIDT K, BRUNNER F & MAYER B 1996 Inhibition of nitric oxide synthesis by NG-nitro-L-arginine methyl ester (L-NAME): requirement for bioactivation to the free acid, NG-nitro-L-arginine. British Journal of Pharmacology, 118,1433–1440. [PubMed: 8832069]

PHILLIPS RG & LEDOUX JE 1992 Differential contribution of amygdala and hippocampus to cued and contextual fear conditioning. Behav Neurosci, 106, 274–85. [PubMed: 1590953]

RAFII S, BUTLER JM & DING BS 2016 Angiocrine functions of organ-specific endothelial cells. Nature, 529, 316–25. [PubMed: 26791722]

RHEE S, KIRSCHEN GW, GU Y & GE S 2016 Depletion of primary cilia from mature dentate granule cells impairs hippocampus-dependent contextual memory. Sci Rep, 6, 34370. [PubMed: 27678193]

SAHAY A, SCOBIE KN, HILL AS, O'CARROLL CM, KHEIRBEK MA, BURGHARDT NS, FENTON AA, DRANOVSKY A & HEN R 2011 Increasing adult hippocampal neurogenesis is sufficient to improve pattern separation. Nature, 472, 466–470. [PubMed: 21460835]

SHEN Q, WANG Y, KOKOVAY E, LIN G, CHUANG SM, GODERIE SK, ROYSAM B & TEMPLE S 2008 Adult SVZ stem cells lie in a vascular niche: a quantitative analysis of niche cell-cell interactions. Cell Stem Cell, 3, 289–300. [PubMed: 18786416]

SONG J, SUN J, MOSS J, WEN Z, SUN GJ, HSU D, ZHONG C, DAVOUDI H, CHRISTIAN KM, TONI N, MING GL & SONG H 2013 Parvalbumin interneurons mediate neuronal circuitry-neurogenesis coupling in the adult hippocampus. Nat Neurosci, 16,1728–30. [PubMed: 24212671]

SONG J, ZHONG C, BONAGUIDI MA, SUN GJ, HSU D, GU Y, MELETIS K, HUANG ZJ, GE S, ENIKOLOPOV G, DEISSEROTH K, LUSCHER B, CHRISTIAN KM, MING GL & SONG H 2012 Neuronal circuitry mechanism regulating adult quiescent neural stem-cell fate decision. Nature, 489,150–4. [PubMed: 22842902]

SUN GJ, ZHOU Y, STADEL RP, MOSS J, YONG JH, ITO S, KAWASAKI NK, PHAN AT, OH JH, MODAK N, REED RR, TONI N, SONG H & MING GL 2015 Tangential migration of neuronal precursors of glutamatergic neurons in the adult mammalian brain. Proc Natl Acad Sci USA, 112, 9484–9. [PubMed: 26170290]

TASHIRO A, MAKINO H & GAGE FH 2007 Experience-specific functional modification of the dentate gyrus through adult neurogenesis: a critical period during an immature stage. J Neurosci, 27, 3252–9. [PubMed: 17376985]

TAVAZOIE M, VAN DER VEKEN L, SILVA-VARGAS V, LOUISSAINT M, COLONNA L, ZAIDI B, GARCIA-VERDUGO JM & DOETSCH F 2008 A specialized vascular niche for adult neural stem cells. Cell Stem Cell, 3, 279–88. [PubMed: 18786415]

TREJO JL, CARRO E & TORRES-ALEMÁN I 2001 Circulating Insulin-Like Growth Factor I Mediates Exercise-Induced Increases in the Number of New Neurons in the Adult Hippocampus. The Journal of Neuroscience, 21, 1628. [PubMed: 11222653]

VAN PRAAG H 2008 Neurogenesis and exercise: past and future directions. Neuromolecular Med, 10, 128–40. [PubMed: 18286389]

WADICHE LO, BROMBERG DA, BENSEN AL & WESTBROOK GL 2005 GABAergic Signaling to Newborn Neurons in Dentate Gyrus .Journal of Neurophysiology, 94, 4528–4532. [PubMed: 16033936]

WANG L, XIA J, YAO J, MASLOV KI & WANG LV 2013 Ultrasonically encoded photoacoustic flowgraphy in biological tissue. Phys Rev Lett, 111, 204301. [PubMed: 24289689]

YUAN SY & RIGOR RR 2010 Regulation of Endothelial Barrier Function. San Rafael (CA).

ZONTA M, ANGULO MC, GOBBO S, ROSENGARTEN B, HOSSMANN KA, POZZAN T & CARMIGNOTO G 2003 Neuron-to-astrocyte signaling is central to the dynamic control of brain microcirculation. Nat Neurosci, 6, 43–50. [PubMed: 12469126]

Highlights

- Hippocampus-engaged exploration induces functional hyperemia in the dentate gyrus
- Functional hyperemia is critical to exploration-induced hippocampal neurogenesis
- Parvalbumin expressing neurons increase blood flow via nitric oxide signaling
- Functional hyperemia elevates IGF-1 pathway activity in the dentate gyrus

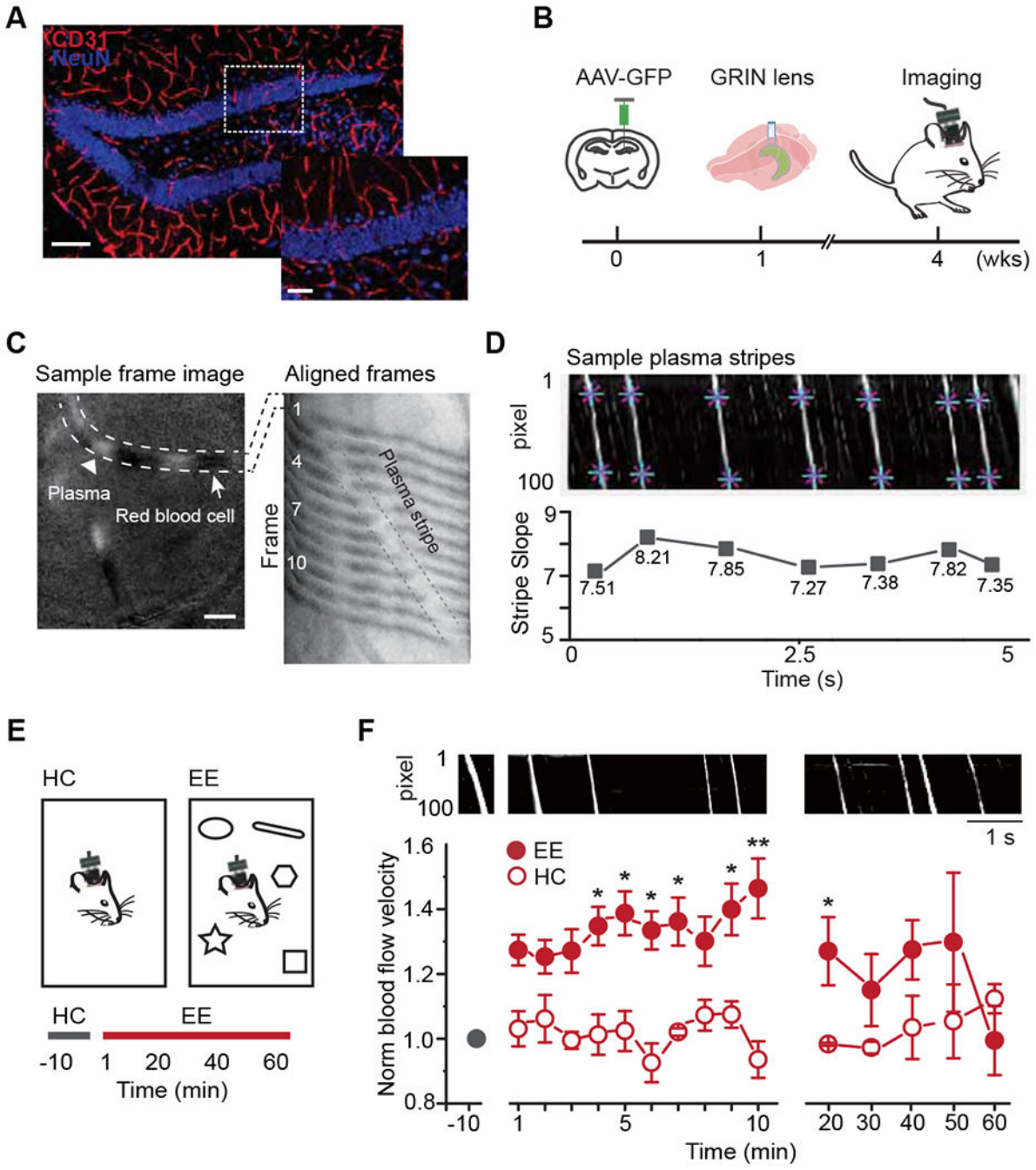

Figure 1. Hippocampus-engaged exploration augmented blood flow velocity in the dentate gyrus

A. The vasculature in the dentate gyrus (red: CD31, blue: NeuN, scale bar: 100 μm). Right is the enlarged image of the region in the white dashed box (scale bar: 40 μm).

B. The experimental procedure and timeline.

C. Microvessels captured by the miniature microscope (left): white dashed lines highlight a microvessel that contains plasma fragments (white, arrow head) and RBC fragments (white, arrow, scale bar: 50 μm). The selected vessel from 12 consecutive frames aligned on one

image to visualize the movement of plasma (right, 80 Hz capturing rate). The plasma formed a white stripe (enclosed by black dashed lines) over time.

D. Sample dynamic map (DMap). An individual white stripe represents an episode of plasma crossing the vessel (eg. C right). The slope of the white stripe represents the blood flow velocity (bottom).

E. Two imaging environments (top) and the recording timeline (bottom).

F. Exploration in EE increased blood flow velocity. DMaps in the HC and EE exploration (top). Normalized blood flow velocity (bottom) in HC (n = 3) and EE for the first 10 min (n = 8, averaged every minute) and the remaining 50 min (n = 4, recorded every 10 min); Linear mixed model for longitudinal data was used for statistical analysis. * P <0.05 and ** P < 0.05/15=0.0033 after Bonferroni adjustment.

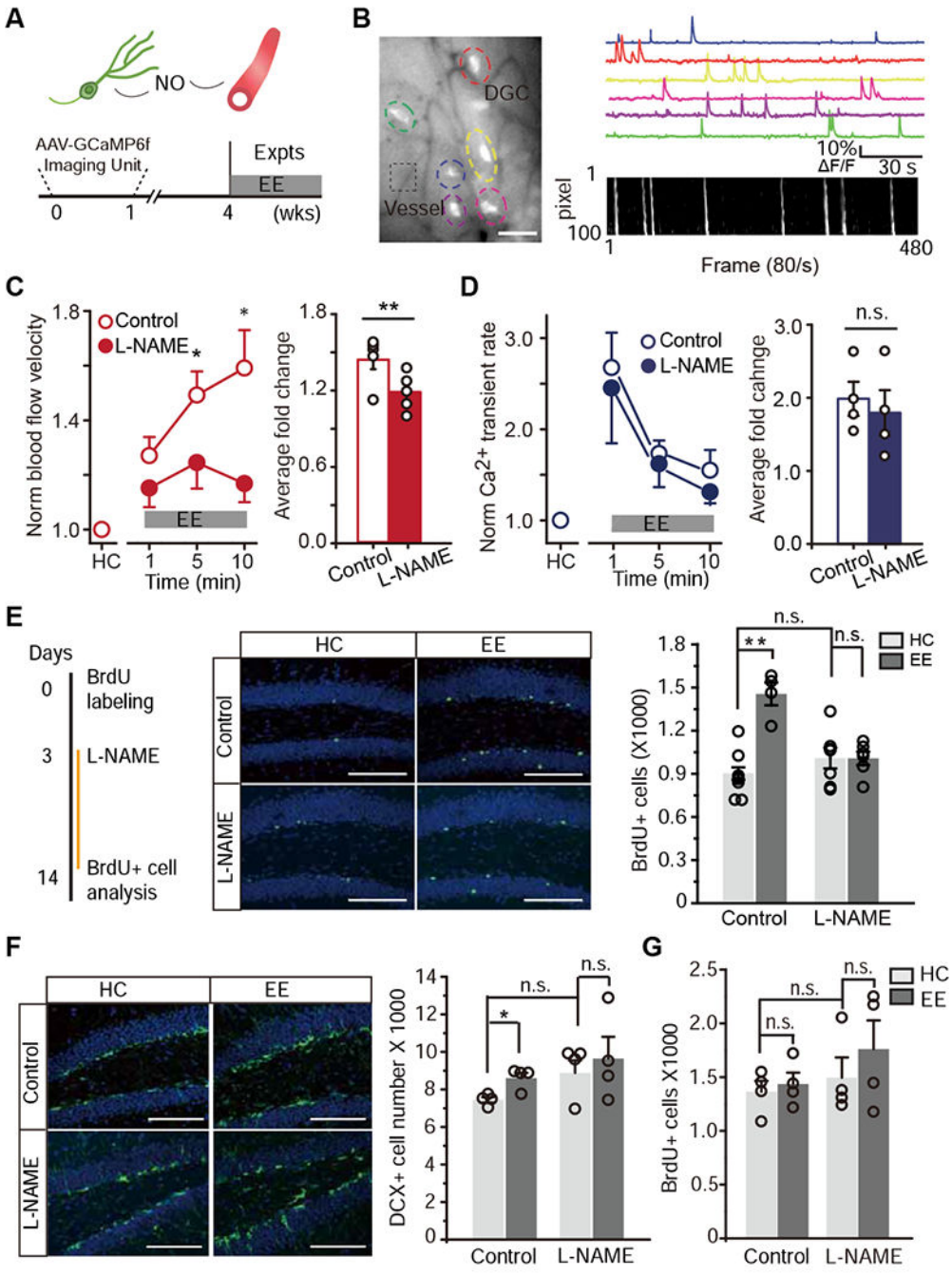

Figure 2. Suppression of the exploration-induced hyperemia dampened activity-dependent hippocampal neurogenesis

A. Schematic model (top). The bottom is the experimental paradigm and timeline.

B. Simultaneous imaging of DGC activity and local blood flow. An imaging with GCaMP6f-labeled DGCs (colored dashed circles) and local microvessels (black dashed box) (left, scale bar: 50 μm). Ca^{2+} signal traces (top right) and DMap (bottom right).

C-D. Inhibition of nNOS attenuated the exploration-induced hyperemia with no detectable effect on DGC activity. C, Normalized blood flow velocity measured from mice with and

without L-NAME administration during HC and EE (left, the velocity was averaged every 3 minutes, Linear mixed model for repeated measurements was used to estimate the differences at each time point. * $P < 0.05$ and ** $P < 0.05/3 = 0.0167$ after Bonferroni adjustment). The average blood flow velocity in each animal is shown for the bar plot (right, n = 5, Wilcoxon signed-rank test was performed using data from all time points, ** $P < 0.01$). D, Normalized Ca^{2+} transient rate from mice with and without L-NAME administration (Same statistical analyses as in **C**, n.s. $P > 0.05$).

E. L-NAME inhibition of nNOS abolished the experience-induced survival of newborn DGCs. The experimental timeline (left). Images of BrdU+ cells at 14 days post BrdU injection (middle, green: BrdU, blue: DAPI, scale bar: 100 μm). The quantification of the number of BrdU+ cells indicating newborn DGC survival (right, n = 8, 4, 7, 6 for each condition, Two-Way ANOVA followed by Bonferroni post hoc test, ** $P < 0.01$, n.s., $P > 0.05$).

F. Images of doublecortin (DCX)+ cells (green: DCX, blue: DAPI) at 14 days post BrdU administration (left). The quantification of average number of DCX+ cells (right, n = 4, same statistical analysis as in **E**, * $P < 0.05$, n.s., $P > 0.05$).

G. Quantification of the average number of BrdU+ cells in the dentate gyrus at 2 days post BrdU administration for every condition (n = 4, n.s., same statistical analysis as in **E**, n.s., P > 0.05).

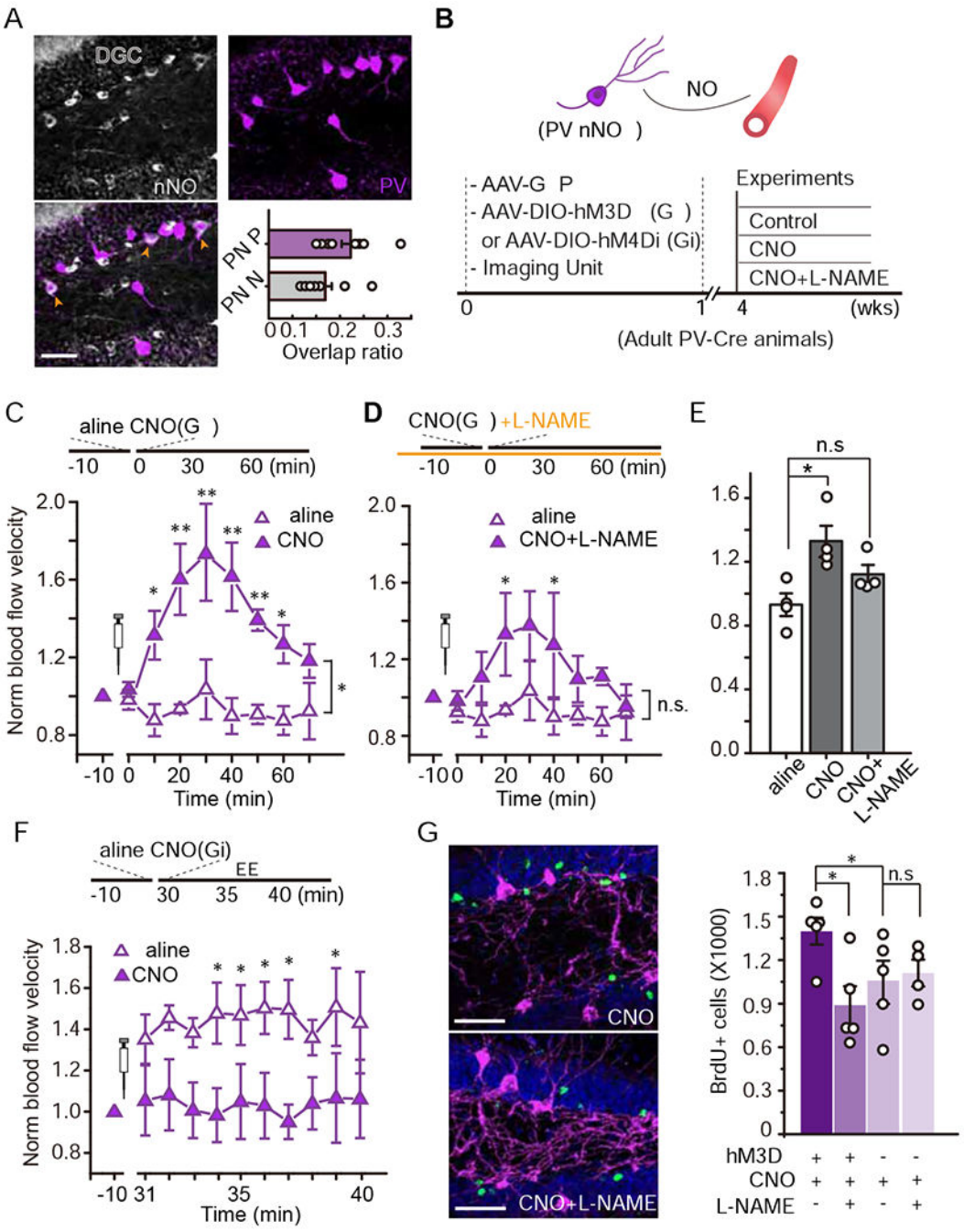

Figure 3. Parvalbumin (PV) neurons mediated neurovascular coupling and promoted experience-induced hippocampal neurogenesis through NO signaling

A. Images of PV (purple) and nNOS (silver) expression in the dentate gyrus. The orange arrow heads indicate cells expressing both cell markers (bottom left, scale bar: 50 μm). The ratios of PV cells expressing nNOS (PN/P) and of nNOS+ cells expressing PV (PN/N) is shown (bottom right, n = 11 brain sections).

B. The hypothetical model (top) and the associated experimental procedure (bottom).

C. Chemogenetic activation (Gq) of PV neurons in the dentate gyrus induced local functional hyperemia. Mice received saline (day 1) and CNO (day 2) while they remained in the HC (n = 4, Linear mixed model for longitudinal data was used to estimate the differences between saline and CNO. * $P < 0.05$, ** $P < 0.05/8 = 0.0063$ after Bonferroni adjustment).
D. The same group of mice received L-NAME-containing water for 24 hr. Blood flow was recorded in the same manner as day 2 with CNO delivery to activate PV neurons (n = 4, same saline data and analysis as those in **C**. * $P < 0.05$, n.s. $P > 0.05$).
E. Quantification of blood flow velocity in saline, CNO, and CNO/L-NAME conditions (Mann-Whitney test, * $P < 0.05$, n.s., $P > 0.05$).
F. Chemogenetic inhibition (Gi) of PV neurons in the dentate gyrus attenuated the exploration-induced functional hyperemia (n = 4, Same analysis as those in **C**. * $P < 0.05$ after Bonferroni adjustment).
G-H. Activation of PV neurons in an nNOS-dependent manner recapitulated experience-induced neurogenesis. G, Images of BrdU+ cells (green: BrdU, purple: PV, and blue: DAPI). H, Quantification of BrdU+ cells in each experimental condition (n = 4, Two-Way ANOVA followed by Bonferroni post hoc test, *$P < 0.05$, n.s. $P > 0.05$).

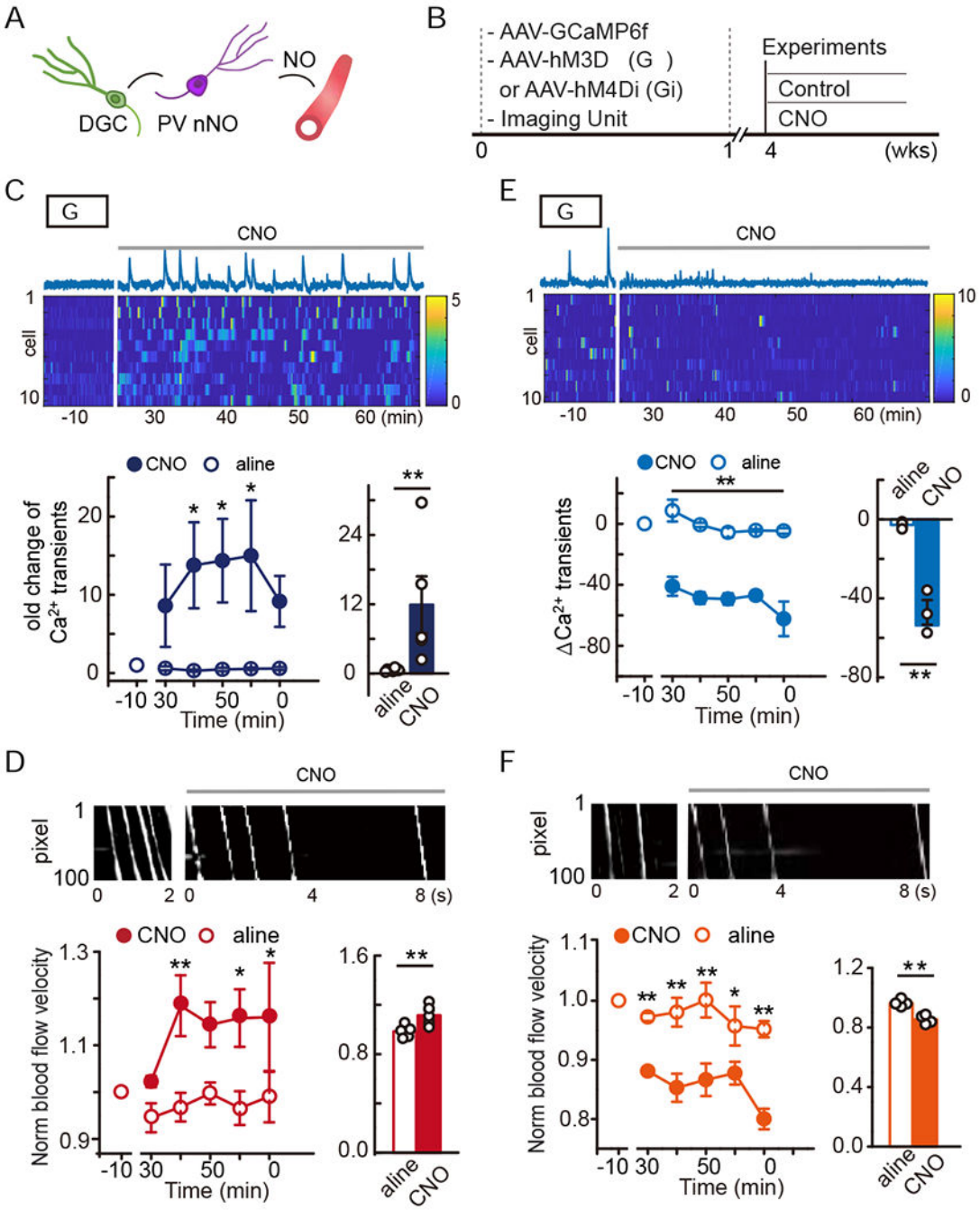

Figure 4. Bidirectional chemogenetic tuning of DGC activity altered local blood flow in the dentate gyrus

A. The hypothetical mode.

B. Simultaneous imaging and chemogenetic manipulation of DGCs.

C-D. hM3Dq activation of DGCs. C, Ca^{2+} trace of a DGC and heatmap of the Ca^{2+} signal intensity from 10 DGCs (top, time 0 indicates CNO delivery). Quantification of DGC activity in terms of Ca^{2+} transient fold change (bottom, n = 5, Linear mixed model for longitudinal data was used to estimate the differences between saline and CNO. * $P < 0.05$;

the average Ca^{2+} transient rate of each animal is shown for the bar plot, Wilcoxon signed-rank test was performed using data from all time points, * $P < 0.05$). **D**, Local microvascular blood flow under hM3Dq activation. Example DMap of the plasma white stripe pre- and post-CNO (top). Quantification of the blood flow velocity pre- and post-CNO (bottom, n = 5, the analyses were similar to those in **C**. * $P < 0.05$, ** $P < 0.05/5 = 0.01$ after Bonferroni adjustment).

E-F. hM4Di inhibition of DGCs. E, the same as C including statistical analyses but with hM4Di manipulation of DGCs (n = 3, * $P < 0.05$, ** $P < 0.05/5 = 0.01$ after Bonferroni adjustment). **F**, The same as D but with hM4Di manipulation (n = 4, * $P < 0.05$, ** $P < 0.05/5 = 0.01$ after Bonferroni adjustment).

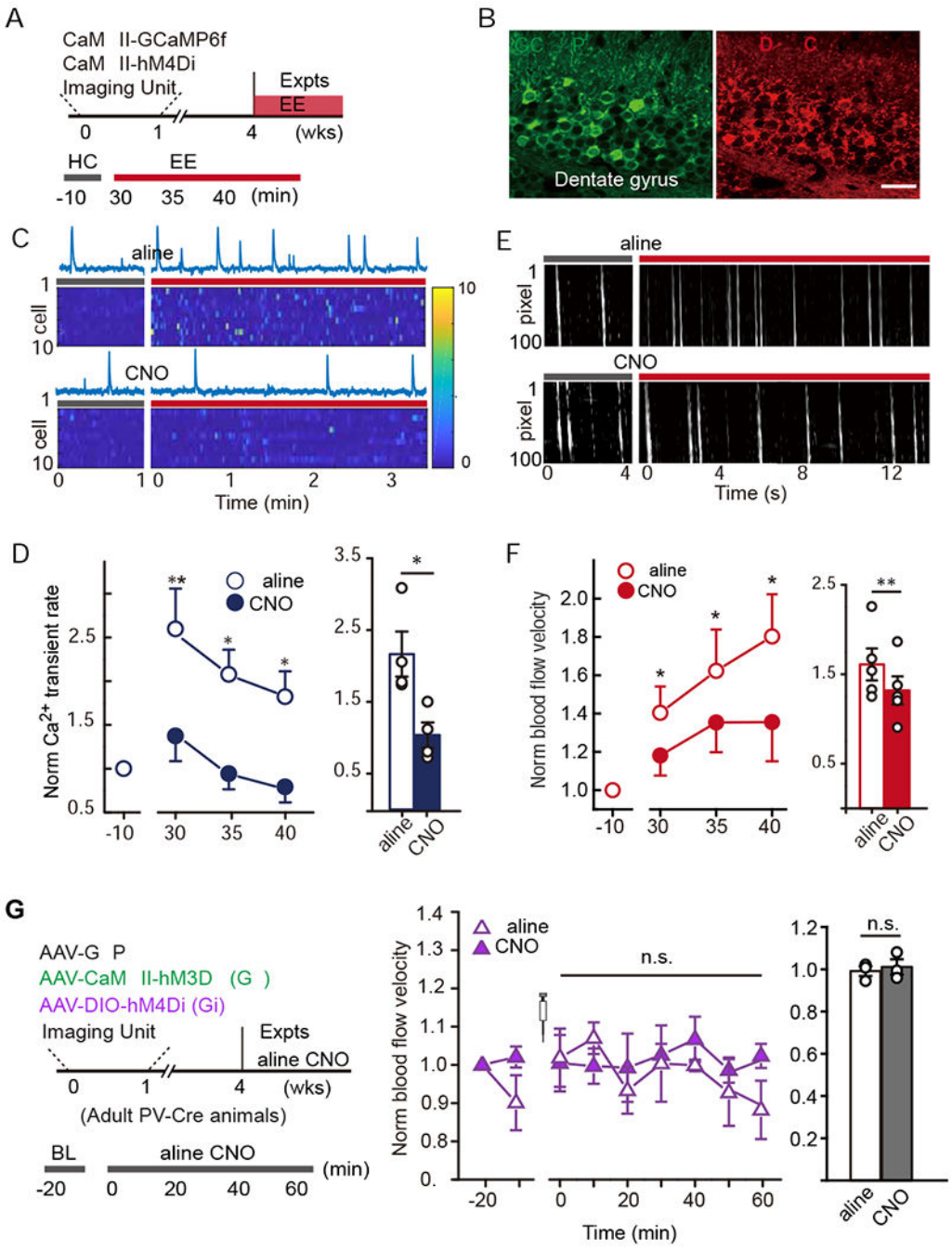

Figure 5. Chemogenetic inhibition of DGC activity dampened exploration-induced hyperemia in the dentate gyrus.

A. Simultaneous imaging and chemogenetic manipulation.

B. Images showing expression of GCaMP6f and hM4Di-mCherry delivery in DGCs. The scale bar is 20 μm,

C-D. Chemogenetic inhibition of DGC activity. C, Sample Ca^{2+} traces of a DGC and heatmap of the Ca^{2+} signal intensity from 10 DGCs pre- and post-EE exploration in control (saline) and CNO conditions. **D**, Normalized Ca^{2+} transient fold change pre- and post-EE

exposure with CNO or saline injections (left). Quantification of the average fold change for each condition (right). n = 4, paired Student's *t*-test, * $P < 0.05$, ** $P < 0.01$.

E-F. The effect of chemogenetic DGC inhibition on exploration-induced hyperemia. E, Sample DMaps with plasma white stripes pre- and post-EE exposure. **F**, Blood flow velocity pre- and post-EE exposure with CNO or saline injection (left). Quantification of the average fold change for each condition (right), n = 5, paired Student's *t*-test, * P < 0.05, ** $P < 0.01$.

G. Experimental design of simultaneous chemogenetic manipulation in DGC and PV neurons.

H. Blood flow velocity for pre- and post- CNO or saline (control) delivery (n= 3, Linear mixed model for longitudinal data was used to estimate the differences between saline and CNO at each time point. n.s. $P > 0.05$; the average blood flow velocity in each animal is shown for the bar plot, Wilcoxon signed-rank test was performed using data from all time points, n.s. $P > 0.05$).

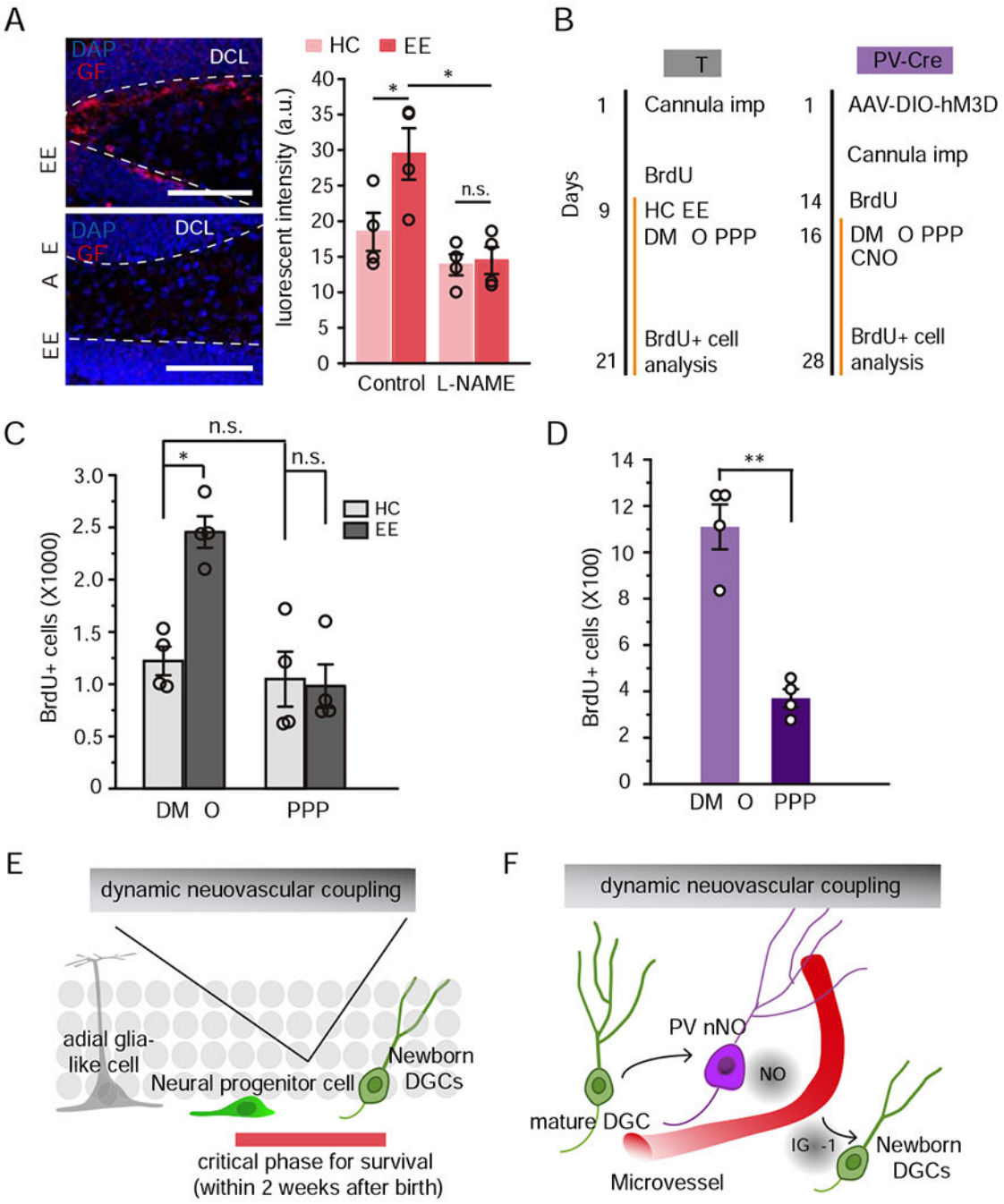

Figure 6. IGF-1/IGF-1R signaling modulated PV-vasculature-induced neurogenesis.

A. Left, phosphorylated IGF-1R immunofluorescent staining in the dentate gyrus after 14-day of EE exploration (Scale bar: 100μm). Right, quantification of the fluorescence intensity of pIGF-1R in each condition (n = 4, Two-Way ANOVA followed by Bonferroni post hoc test, * $P < 0.05$, n.s., $P > 0.05$).

B. Experimental timeline of neurogenesis assessment with IGF-1R antagonist infusion (PPP) in WT (left) and PV-Cre (right) mice.

C. Quantification of the number of BrdU+ cells in the dentate gyrus of PV mice indicating newborn DGC survival in each condition (right, n = 4 for each condition, Two-Way ANOVA followed by Bonferroni post hoc test, * $P < 0.05$, n.s., $P > 0.05$).

D. Quantification of the number of BrdU+ cells in the dentate gyrus of PV-Cre mice indicating newborn DGC survival in each condition (right, n = 4 for each condition, Kruskal-Wallis test, * $P < 0.05$).

E. Dynamic neurovascular coupling regulates newborn DGC survival.

F. Communication between DGCs, PV-expressing interneurons, and the vasculature.

KEY RESOURCES TABLE

REAGENT or RESOURCE	SOURCE	IDENTIFIER
Antibodies		
Rat anti-BrdU	Abcam	Cat# ab6326, RRID: AB_305426
Goat anti-doublecortin	Santa Cruz	Cat# sc-8066, RRID: AB_2088494
Mouse anti-NOS1	Santa Cruz	Cat# sc-5302, RRID: AB_626757
Rabbit anti-parvalbumin	Abcam	Cat#: 11427, RRID: AB_298032
Mouse anti-NeuN	MilliporeSigma	Cat# MAB377, RRID: AB_2298772
Rat anti-CD31	BD Biosciences	Cat# 557355, RRID: AB_396660
Rabbit anti-Cleaved Caspase-3	Cell Signaling	Cat# 9664, RRID: AB_2070042
Bacterial and Virus Strains		
AAV9.CamKII.GCaMP6f.WPRE.SV40	Penn Vector Core/Addgene	Cat# 100834-AAV9
AAV8-CaMKIIa-EGFP	Addgene	Cat# 50469-AAV8
AAV8-CaMKIIa-hM3Dq-mCherry	Addgene	Cat# 50476-AAV8
AAV8-CaMKIIa-hM4Di-mCherry	Addgene	Cat# 50477-AAV8
AAV8-hSyn-DIO-hM3Dq-mCherry	Addgene	Cat# 44361-AAV8
AAV8-hSyn-DIO-hM4Di-mCherry	Addgene	Cat# 44362-AAV8
AAV8-hSyn-DIO-mCherry	Addgene	Cat# 50459-AAV8
AAV8-GFP-U6-m-NOS1-shRNA	Vector Biolabs	Cat# shAAV-279053
AAV8-GFP-U6-scrmb-shRNA	Vector Biolabs	Cat# AAV8-GFP-U6-scrmb-shRNA
Chemicals, Peptides, and Recombinant Proteins		
5-bromo-2′-deoxyuridine (BrdU)	Sigma	Cat# B5002
Clozapine-N-oxide (CNO)	Enzo Life Sciences	Cat# BML-NS105-0005
N omega-nitro-L-arginine methyl ester (L-NAME)	Sigma	Cat# N5751
Picropodophyllotoxin (PPP)	Cayman Chemical Company	Cat# 17329
Experimental Models: Organisms/Strains		
Mouse: PV-Cre	Jackson Laboratory	stock# 017320